International Communications in Heat and Mass Transfer 116 (2020) 104634

Contents lists available at ScienceDirect

International Communications in Heat and Mass Transfer

journal homepage: www.elsevier.com/locate/ichmt

Thermal and hydrodynamic behavior of suspensions comprising nano-encapsulated phase change materials in a porous enclosure

Ali Tahmasebi[a], Hossein Zargartalebi[b], S.A.M. Mehryan[c], Mohammad Ghalambaz[d,e,*]

[a] Department of Mechanical Engineering, Shahid Chamran University of Ahvaz, Ahvaz, Iran.
[b] Department of Mechanical and Manufacturing Engineering, Centre for Bioengineering Research and Education, University of Calgary, Calgary, Canada
[c] Young Researchers and Elite Club, Yasooj Branch, Islamic Azad University, Yasooj, Iran
[d] Metamaterials for Mechanical, Biomechanical and Multiphysical Applications Research Group, Ton Duc Thang University, Ho Chi Minh City, Vietnam
[e] Faculty of Applied Sciences, Ton Duc Thang University, Ho Chi Minh City, Vietnam

ARTICLE INFO

Keywords:
NEPCMs
Nanoencapsulation
Porous medium
Stefan number
Fusion temperature

ABSTRACT

Nano-encapsulated phase change materials (NEPCMs) are known to enhance the thermal characteristics of fluids; therefore, there is a rising interest in employing these materials in future thermal control systems. This paper investigates hydrodynamic and thermal characteristics of nanofluids, NEPCMs mixed in the host liquid, in glass balls as a porous structure. The geometry is a two-dimensional porous square cavity in which the left boundary is hot, the right boundary is cold, and the horizontal ones are considered to be insulated. The NEPCMs are composed of polyurethane (PU) as shell and nonadecane as a core. The impact of different non-dimensional parameters, such as Darcy number, $10^{-5} \le Da \le 10^{-1}$, porosity, $0.4 \le \varepsilon \le 0.9$, Stefan number, $0.2 \le Ste \le 100$, fusion temperature, $0 \le \theta_f \le 1$, and volume fraction of the NEPCMs, $0 \le \phi \le 0.05$, is studied on the flow and heat transfer characteristics. It is shown that the volume fraction of NEPCMs is directly proportional to the strengthening of the heat transfer rate in such a way that applying 5% volume fraction of NEPCMs could enhance the heat transfer up to 20.1% and 14.1% at $\theta_f = 0.5$ in comparison to the cases of pure fluid and NEPCM mixture with no core-phase change, respectively. The effect of non-dimensional fusion temperature on the rate of heat transfer is also found to be noticeable. The maximum average Nusselt number emerges at $\theta_f = 0.5$, which is the optimum fusion temperature.

1. Introduction

Buoyancy-induced heat transfer in a cavity is a fundamental and important problem attracting great attention of many researchers in academia and industry due to its central applications, including nuclear reactors, solar thermal collector platforms, and geothermal systems [1–4]. The physics of porous structures are also interesting in some applications, such as solar power collectors and the underground pollutants diffusion. In essence, the mechanical systems due to deficiencies in the external power supply are almost ill-fated, and the lack of an appropriate and well-established natural convection platform as a reliable alternative to these systems has been highlighted. These convective systems also noticeably decrease the induced noise of fans in mechanical systems. Therefore, owing to the aforementioned virtues, many researchers are fascinated by natural convection [5,6] or mixed convection [7] in porous media. Various aspects of heat transfer have also been investigated in porous media, including thermal stratification [8], mass transport [9], heat generation [10], and magnetic field effects [11].

Moreover, experiments on the thermophysical characteristics of nanofluids reveal that due to the presence of tiny nano-particles in the base fluid, the thermophysical properties, comprise heat capacity, density, and dynamic viscosity of the suspension are influenced [12]. NEPCMs are a special kind of materials composed of two-part nano-particle, a shell which covers a core. The nucleus component proves a Phase Change Material (PCM) that could be liquid or solid depending on the amount of temperature, which either releases or absorbs a huge proportion of energy because of the latent heat of fusion [13,14]. Researchers have synthesized multifarious types of nano/micro-encapsulated PCM suspensions such as formaldehyde polymer as a shell encapsulating n-tetradecane [15], melamine formaldehyde shell and 5 wt% styrene–maleic anhydride–monomethyl (SMA) as an emulsifier with tetradecane core [16], n-Eicosane coated with PMMA as a shell [17], n-Octadecane coated with Polystyrene [18,19], and n-Octadecane core covered with methyl methacrylate (MMA)-based polymer [20] to name but a few. Thorough studies on micro/nano capsulation of PCMs have been performed recently [13,21].

* Corresponding author at: Ton Duc Thang University, Ho Chi Minh City, Vietnam.
E-mail address: mohammad.ghalambaz@tdtu.edu.vn (M. Ghalambaz).

https://doi.org/10.1016/j.icheatmasstransfer.2020.104634

Available online 30 June 2020

Several platforms can be found in industry, including detectors, microchips, and laser optical alignment systems in which non-uniform temperature gradients or temperature rises can easily affect their performance. These devices desire an accurate approach to control the temperature. Hence, NEPCMs are promising alternatives to classical approaches for regulating the temperature of working fluids and consequently enhance the performance cooling systems. Engineers have employed PCMs and nano-enhanced PCMs for several industrial and technological applications, especially for thermal energy storage [22], such as buildings thermal management [23,24], thermal storage of solar energy [25], and short term storage using the domestic heat pump and air-conditioning platforms [26]. PCMs are known as materials with high capability of storing/releasing a large energy value during phase change; however, when it comes to heat transfer, these materials show very weak performance. Therefore, improvement of the PCM heat transfer properties has been the target of many researchers employing, for example, porous structure or metallic fins [27–29]. In this regard, nanoparticles have been used by several researchers to increase heat transfer and phase change phenomenon in PCMs [23,30,31]. The nanoparticles in some other cases have been added to PCMs, known as Nano-Enhanced Phase Change Materials, as additives to intensify heat transfer properties [30,32,33]; on the contrary, the term NEPCM represents a phase change core which coated with a nano-capsule shell suspended in a working fluid.

The researches regarding NEPCMs heat transfer are almost restricted to forced convection phenomenon in ducts, tubes, and micro/mini-channels to name but a few. For example, Seyf et al. [34] numerically investigated the forced convection phenomenon in a mixture of octadecane NEPCMs (100 nm) and base water over an isothermal cylinder. Considering flow to be steady and laminar regime, they performed a parametric investigation for various volume fractions of nanoparticles. In another study, they, presenting a three-dimensional model, theoretically investigated heat and fluid flow parameters affecting micro-tube heat sink using NEPCMs as coolant. They found that nanoparticles positively affect the heat transfer and consequently cooling capability of the studied liquid is enhanced, but they experienced a huge pressure drop across the tube due to the presence of the particles [35].

Ho et al. [36] studied the pressure drop as well as cooling performance of a minichannel heat sink saturated with encapsulated phase change microparticles. They observed that in a couple of particular examples, cooling performance could be enhanced up to 52%, but in a few other examples, they reported that heat transfer is declined. There are also some experimental investigations comparing the heat transfer amendment employing regular Al2O3 nanoparticles or a mixture of PCMs into minichannel heat sink [37] and circular tubes [38]. There is no consensus in heat transfer behavior due to the fact that different parameters, including a heating position in the system and the rate of flow, can affect the heat transfer performance, and as a result, no general conclusion can be drawn. However, Ghalambaz et al. [39] recently performed a study of natural heat convection of NEPCMs in an enclosure. They reported that one of the effective factors, which influences heat transfer augmentation is the fusion temperature of the NEPCMs . Hajjar et al. [40] also explored the unsteady heat transfer of NEPCMs in a cavity enclosure. They found that using 2.5% of NEPCMs particles can improve heat transfer by 21%. Considering heat transfer of NEPCMs in a porous space, there Ghalambaz et al. [41] investigated the mixed convection heat transfer of phase change nanoparticles placed over a vertical flat plate. They used a boundary layer approach and found that the decline of fusion temperature of nanoparticles improves the heat transfer.

The motivation behind this study is to investigate natural convection flow and heat transfer in a square enclosure containing porous structure saturated with a nanofluid, as a low-concentration suspension of a host fluid and NEPCMs. It is worth mentioning that, to the best of the author's knowledge, the natural convection of NEPCMs in a porous enclosure has not been addressed yet. The central results of this research could be of interest in future platforms regarding thermal control systems including encapsualted nanoparticles as the phase change materials.

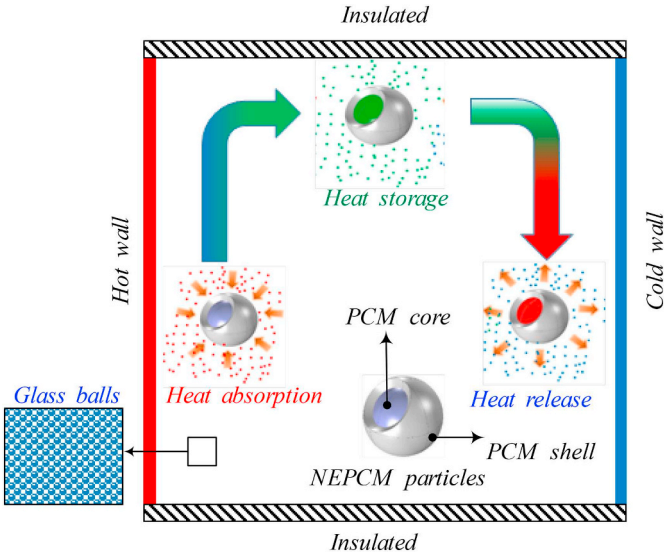

Fig. 1. Schematic configuration of the problem physics.

2. Physics and modeling

2.1. Physical model

The geometry considered is a 2D porous medium enclosed (shown in Fig. 1), with glass spheres as the solid matrix. The void space between the glass spheres is occupied with a dilute suspension in which water is the host liquid and the particles of NEPCMs are nano-additives. The shell of the nano-additives is polyurethane (PU) and its core is nonadecane. The left of the chamber is heated at a temperature of T_h above the right side with T_c temperature, while the other walls of the enclosure are thermally impervious. The Biot number of NEPCM particles is very low as the characteristic size of the particles is very small, and hence, they are modeled as lamped particles, and also the density change of nanoparticles on phase change is neglected.

There exists no heat transfer between the solid matrix and fluid phase in the porous structure. Table 1 lists the thermo-physicalcharacteristics of the host liquid, nano-additives, and the solid matrix. The melting point temperature of the core is 32 °C, and its latent heat is 211 kJ/kg [42].

2.2. The mathematical model

The equations of conservation of mass, momentum and energy for a mixture including NEPCM particles under the foregoing assumptions are as follows:

Continuty equation:

Table 1
Thermophysical properties of the host fluid, NEPCM particles and solid matrix [42,43].

Material	μ (kg/m.s)	C_p (J/kg.K)	ρ (kg/m^3)	β (K^{-1})	k (W/m.K)
Water	8.9×10^{-4}	4179	997.1	21×10^{-5}	0.613
Polyurethane	–	1317.7	786	17.28×10^{-5}	
Nonadecane	–	2037	721		
Glass balls	–	840	2700	0.9×10^{-5}	1.05

$$\frac{\partial v}{\partial y} + \frac{\partial u}{\partial x} = 0 \tag{1}$$

Momentum equation:

$$\frac{\rho_b}{\varepsilon^2}\left(v\frac{\partial u}{\partial y} + u\frac{\partial u}{\partial x}\right) = -\frac{\partial p}{\partial x} + \frac{\mu_b}{\varepsilon}\left(\frac{\partial^2 u}{\partial y^2} + \frac{\partial^2 u}{\partial x^2}\right) - \frac{\mu_b}{K}u \tag{2-a}$$

$$\frac{\rho_b}{\varepsilon^2}\left(v\frac{\partial v}{\partial y} + u\frac{\partial v}{\partial x}\right) = -\frac{\partial p}{\partial y} + \frac{\mu_b}{\varepsilon}\left(\frac{\partial^2 v}{\partial y^2} + \frac{\partial^2 v}{\partial x^2}\right) + g\rho_b\beta_b(T - T_c) - \frac{\mu_b}{K}v \tag{2-b}$$

Energy equation:

$$(\rho C_p)_b\left(v\frac{\partial T}{\partial y} + u\frac{\partial T}{\partial x}\right) = k_{m,b}\left(\frac{\partial^2 T}{\partial y^2} + \frac{\partial^2 T}{\partial x^2}\right) \tag{3}$$

where

$$k_{m,b} = k_s + \varepsilon(k_b - k_s) \tag{4}$$

b is the characteristics of the suspension, *m* denotes the characteristics of the porous medium, and *s* denotes the characteristics of the solid matrix. Regarding the schematic view of the geometry, the mathematical form of the boundary conditions are:

$$T(0y) = T_h,\ u(0, y) = v(0, y) = 0 \tag{5-a}$$

$$T(H, y) = T_c,\ u(H, y) = v(H, y) = 0 \tag{5-b}$$

$$\frac{\partial T(x, 0)}{\partial y} = 0,\ u(x, 0) = v(x, 0) = 0 \tag{5-c}$$

$$\frac{\partial T(x, H)}{\partial y} = 0,\ u(x, H) = v(x, H) = 0 \tag{5-d}$$

2.3. The suspension thermo-physical properties

The effective density of the suspension is calculated based onthe densities of water and NEPCM particles and the concentration of particles can be written as the following [44]:

$$\rho_b = (1 - \phi)\rho_f + \phi\rho_p \tag{6}$$

The subscript *p* denotes the characteristics of the nano-additives and subscript *f* denotes the characteristics of the host liquid. The density of the particles of NEPCMs is evaluated as the following [44,45]:

$$\rho_p = \frac{(1 + \iota)\rho_{co}\rho_{sh}}{\rho_{sh} + \iota\rho_{co}} \tag{7}$$

ρ_{sh} is the denisty of the shell of the nano-additives and ρ_{co} is the density of the core of the nano-additives. ι, the core to the shell weight ratio, is about $\iota \sim 0.447$ [42]. The mixture heat capacity is a function of the heat capatities of the host liquid and the nano-additives, concentration of the nano-additives, and density of the mixture [45,46]:

$$C_{p,b} = \rho_f\rho_b^{-1}C_{p,f}(1 - \phi) + \rho_p\rho_b^{-1}C_{p,p,eff}\phi \tag{8}$$

$C_{p,p,eff}$ is the effective heat capacity of the nano-additives which is equal to its sensible heat capacity, i.e. $C_{p,p}$, in the cases that the core of the NEPCMs particles does not experience the phase change. By taking into consideration the core phase change of the particles, the heat capacity of the NEPCMs can be modeled using one of the following functions [35,44]:

$$C_{p,p,eff} = T_{Mr}^{-1}(T - T_0)h_{sf} + C_{p,p} \tag{9-a}$$

$$C_{p,p,eff} = \left\{\frac{\pi}{2}\cdot(h_{sf}T_{Mr}^{-1} - C_{p,p})\cdot\sin(T_{Mr}^{-1}\pi(T - T_0))\right\} + C_{p,p} \tag{9-b}$$

$$C_{p,p,eff} = 2(T_{Mr}^{-2}h_{fs} - T_{Mr}^{-1}C_{p,p})(T - T_0) + C_{p,p} \tag{9-c}$$

In which T_{Mr}, the temperature melting range, is:

$$T_{Mr} = T_1 - T_0 \quad \begin{vmatrix} T_0 = T_f - T_{Mr}/2 \\ T_1 = T_f + T_{Mr}/2 \end{vmatrix} \tag{10}$$

The core of the particles melts when the temperature is between T_0 and T_1. Hence, based on the sinusoidal profile of the heat capacity, we then have:

$$C_{p,p,eff} = C_{p,p} + \left\{\frac{\pi}{2}\cdot(h_{sf}T_{Mr}^{-1} - C_{p,p})\cdot\sin(T_{Mr}^{-1}\pi(T - T_0))\right\} \times \begin{cases} 0 & T < T_0 \\ 1 & T_0 < T < T_1 \\ 0 & T > T_1 \end{cases} \tag{11}$$

The coefficient of thermal volume-expansion of the mixture is [46]:

$$\beta_b = (1 - \phi)\beta_f + \phi\beta_p \tag{12}$$

In the literature [47,48], the effect of various parameters of nanofluids, such as shape, type, and size of nanoparticles, type of the base fluid and the working temperature on the dynamic viscosity and thermal conductivity of nanofluids was summarized in two parameters of dynamic viscosity number and thermal conductivity number. These two numbers can be estimated using experimental data. The following relations can be employed to obtain the dynamic viscosity and thermal conductivity of the suspension:

$$\frac{\mu_b}{\mu_f} = 1 + Nv\phi \tag{13-a}$$

$$\frac{k_b}{k_f} = 1 + Nc\phi \tag{13-b}$$

Nc and *Nv*, respectively, are the numbers of dynamic viscosity and thermal conductivity. The utilized relations for obtaining the effective thermal conductivity and viscosity are admissible when $\phi \leq 5\%$.

2.4. Normalizing the governing equations

To normalize the Eqs. (1)–(4) as well as the imposed boundary conditions, i.e. Eq. (5), the following variations are utilized:

$$X = \frac{x}{H},\ Y = \frac{y}{H},\ U = \frac{uH}{\alpha_f},\ V = \frac{vH}{\alpha_f},\ P = \frac{pH^2}{\rho_f\alpha_f^2},\ \theta = \frac{T - T_c}{\Delta T} \tag{14}$$

Where $\Delta T = T_h - T_c$. Hence, we then have:

$$\frac{\partial V}{\partial Y} + \frac{\partial U}{\partial X} = 0 \tag{15}$$

$$\varepsilon^{-2}\left(\frac{\rho_b}{\rho_f}\right)\left(V\frac{\partial U}{\partial Y} + U\frac{\partial U}{\partial X}\right) = -\frac{\partial P}{\partial X} + Pr\varepsilon^{-1}\left(\frac{\mu_b}{\mu_f}\right)\left(\frac{\partial^2 U}{\partial Y^2} + \frac{\partial^2 U}{\partial X^2}\right) - \frac{Pr}{Da}\left(\frac{\mu_b}{\mu_f}\right)u \tag{16}$$

$$\varepsilon^{-2}\left(\frac{\rho_b}{\rho_f}\right)\left(V\frac{\partial V}{\partial Y} + U\frac{\partial V}{\partial X}\right) = -\frac{\partial P}{\partial Y} + Pr\varepsilon^{-1}\left(\frac{\mu_b}{\mu_f}\right)\left(\frac{\partial^2 V}{\partial Y^2} + \frac{\partial^2 V}{\partial X^2}\right) + Ra\cdot Pr\left(\frac{\beta_b}{\beta_f}\right)\left(\frac{\rho_b}{\rho_f}\right)\theta - \frac{Pr}{Da}\left(\frac{\mu_b}{\mu_f}\right)v \tag{17}$$

The parameters in Eqs. (16)-(17), the Rayleigh (*Ra*), the Prandtl (*Pr*), and the Darcy (*Da*) numbers, are:

$$Ra = \frac{g\rho_f\beta_f\Delta TH^3}{\alpha_f\mu_f},\ Pr = \frac{\mu_f}{\rho_f\alpha_f},\ Da = \frac{K}{H^2} \tag{18}$$

We assume that NEPCM particles and the base fluid volumetrically expand in the same way; therefore, the thermal expansion ratio could be approximated as $\beta_b/\beta_f \sim 1$. Furthermore, since the value of density ratio for $\phi = 5\%$ is 0.987, this ratio is considered to be 1 for the bouancy term.

Table 2
Grid independence examination for the *Nu* and the $|\Psi|_{max}$.

Grid size	*Nu*	$\Delta = \frac{\lvert Nu_{i\times j} - Nu_{150\times150}\rvert}{Nu_{i\times j}} \times 100$	$\lvert\Psi\rvert_{max}$	$\Delta = \frac{\lvert \Psi_{i\times j} - \Psi_{150\times150}\rvert}{\Psi_{i\times j}} \times 100$
100 × 100	8.8278	0.007	13.535	0.015
150 × 150	8.8284	–	13.537	–
200 × 200	8.8287	0.003	13.538	0.007
250 × 250	8.8288	0.005	13.539	0.015
300 × 300	8.8291	0.008	13.539	0.015

$$Cr\left(V\frac{\partial\theta}{\partial Y} + U\frac{\partial\theta}{\partial X}\right) = \left(\frac{k_{m,b}}{k_f}\right)\left(\frac{\partial^2\theta}{\partial Y^2} + \frac{\partial^2\theta}{\partial X^2}\right) \tag{19}$$

where

$$Cr = \frac{(\rho C_p)_b}{(\rho C_p)_f} = (1-\phi) + \phi\lambda + \frac{\phi}{\delta\, Ste} f \tag{20-a}$$

$$\frac{k_{m,b}}{k_f} = (1-\varepsilon)\frac{k_s}{k_f} + \varepsilon(1 + Nc\phi) \tag{20-b}$$

Cr denotes the normalized heat capacity of the mixture,which is a function of the heat capacity of the base liquid. As previously raised, *Cr* of suspension containing the NEPCMs particles involves the latent heat of NEPCM's core when melting the cores. The first two terms on the right side of Eq. (20-a) point out the sensible heat of the suspension and the other one shows the latent heat effects on the heat capacity of the suspension. The normalized melting interval (δ), the heat capacity ratio (λ) and the Stefan number (*Ste*) are, respectively:

$$\delta = \frac{T_{Mr}}{\Delta T},\ \lambda = \frac{(C_{p,c,l} + \iota C_{p,s})\rho_c\rho_s}{(\rho C_p)_f(\rho_s + \iota\rho_c)},\ Ste = \frac{\Delta T(\rho_s + \iota\rho_c)(\rho C_p)_f}{h_{sf}\rho_c\rho_s} \tag{21}$$

Also, the normalized fusion function, i.e *f*, is:

$$f = \frac{\pi}{2}\sin\left(\frac{\pi}{\delta}\left(\theta - \theta_f + \frac{\delta}{2}\right)\right) \times \begin{cases} 0 & \theta < \theta_f - \delta/2 \\ 1 & \theta_f - \delta/2 < \theta < \theta_f + \delta/2 \\ 0 & \theta > \theta_f + \delta/2 \end{cases} \tag{22}$$

where θ_f, the dimensionless fusion temperature, is.

$$\theta_f = \frac{T_f - T_c}{\Delta T} \tag{23}$$

The boundary conditions in the dimensionless space are:

$$U(0,Y) = V(0,Y) = 0,\ \theta(0,Y) = 1 \tag{24-a}$$

$$U(1,Y) = V(1,Y) = 0,\ \theta(1,Y) = 0 \tag{24-b}$$

$$U(X,0) = V(X,0) = 0,\ \frac{\partial\theta(X,0)}{\partial Y} = 0 \tag{24-c}$$

$$U(X,1) = V(X,1) = 0,\ \frac{\partial\theta(X,1)}{\partial Y} = 0 \tag{24-d}$$

2.5. Heat transfer rate and stream function

The local heat transfer rate through the hot surface is obtained by the use of the relation given below:

$$Nu_Y = -\left[(1-\varepsilon)\frac{k_s}{k_f} + \varepsilon(1 + Nc\phi)\right]\left(\frac{\partial\theta}{\partial X}\right)_{Y=0} \tag{25}$$

Integrating the Eq. (25) gives the total heat transfer rate:

$$Nu = \int_0^1 Nu_Y\, dY \tag{26}$$

Also, to visualize the suspension flow, we drew the streamlines by solving the following Poisson equation:

$$\frac{\partial^2\Psi}{\partial X^2} + \frac{\partial^2\Psi}{\partial Y^2} = -\left(\frac{\partial V}{\partial X} - \frac{\partial U}{\partial Y}\right) \tag{27}$$

On the walls, $\Psi = 0$.

3. Numerical approach and grid test

The normalized governing equations under the imposed boundary conditions were discretized by the use of a weighted finite element approach. The steep temperature and velocity gradients were solved by the use of a non-uniform structure grid. To fully couple the controling discretized equations, the damped newton method was utilized . Finally, Parallel Sparse Direct Solver is employed to achieve the solution for the corresponding linear algebraic equations. The stopping criterion of 10^{-5} was applied for all dependent variables. Ref. [49] describes the employed numerical approach, in detail.

The utilized mesh in the study domain is a quadratic non-uniform structured grid. Equal mesh points (*m*) are considered for the horizontal and vertical walls. Therefore, the computational domain has a grid size of $m \times m$. As tabulated in Table 2, several grids of different sizes are analyzed to find the proper grid size. The results of grid independence examination for the average Nusselt number and the maximum velocity inside the porous medium are showed for the studied grids when $Ra = 10^6$, $Da = 10^{-3}$, $Pr = 6.2$, $Ste = 0.2$, $\theta_f = 0.2$, $\phi = 0.05$, $\varepsilon = 0.65$, $Nc = 23.8$, $Nv = 12.5$, $\lambda = 0.333$, and $\delta = 0.05$. The grids generated near the boundaries of the mediumare denser by utilizing a stretching ratio of 10, for the gradients of temperature and velocity are significantly high in these regions. Therefore, considering the computational cost and the accuracy, the non-uniform grid size of 150 × 150 inside the domain has been selected for the ensuing analysis

To verify the numerical approach utilized in this work, the current numerical predictions can be compared with the results previously reported in [50–53]. Tables 3 and 4, and Fig. 2 present theses comparisons. As clearly seen, the developed code is correct and accurate.

4. Results and discussion

In this portion, the effects of different involved parameters on the heat transfer rate and governing fields are numerically explored. The *Nc* and *Nv* parameterscan be considered to be 23.8 and 12.5, respectively. As previously mentioned, PU-nonadecane NEPCMs are employed as nanoparticles. It is worth noting that if the suspension is dilute (i.e., $0 \le \phi \le 5\%$), the values above presented are usable. Besides, the sensible heat capacity ratio (λ) reported by Barlak et al. [42] is 0.333. Moreover, the values of the Rayleigh number (*Ra*) and the Prandtl number (*Pr*) are considered to be constant so that $Ra = 10^6$ and $Pr = 6.2$. We assume thatthe non-dimensional parameters have default

Table 3
Comparison of the results (*Nu*) of the developed code and the results reported by Kahveci et al. [50] for $Ra = 10^6$.

Work	$\phi = 0$	$\phi = 0.05$	$\phi = 0.1$
Kahveci et al. [50]	9.23	9.783	10.297
Present study	9.20	9.76	10.3

Table 4
The *Nu* in a porous medium filled with a suspension of water and nano-additives of Cu when $Da \times Ra = 10^3$

ϕ	Present work	Sheremet et al. [52]	Sun and Pop [51]
0.1	9.42	9.41	9.42
0.2	12.85	12.84	12.85

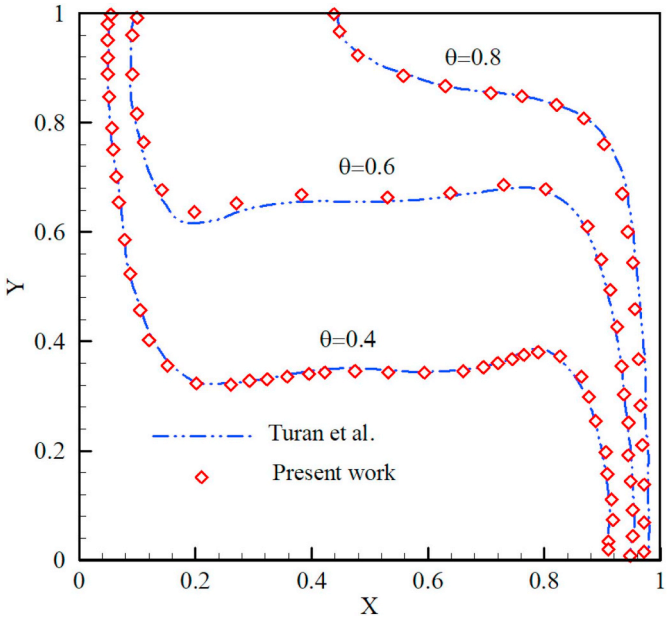

Fig. 2. The temperature fields of the developed code in this work and and acquired by Turan et al. [53] for $Ra = 10^5$, $\phi = 0.0$, and $Pr = 1000$.

values of $Ra = 10^6$, $Da = 10^{-3}$, $Pr = 6.2$, $Ste = 0.2$, $\theta_f = 0.2$, $\phi = 0.05$, $\varepsilon = 0.65$, $Nc = 23.8$, $Nv = 12.5$, $\lambda = 0.333$, and $\delta = 0.05$. The results extraction is executed based on the aforementioned values. In the cases of studying the variations of the non-dimensional parameters, the changes in the default values will be expressed.

The numerical investigation is performed for the five types of influential non-dimensional parameters consisting of the Darcy number ($10^{-5} \le Da \le 10^{-1}$), the porosity ($0.4 \le \varepsilon \le 0.9$), the volume fraction of the NEPCM particles ($0 \le \phi \le 0.05$), the non-dimensional fusion temperature ($0 \le \theta_f \le 1$), and the Stefan number ($0.2 \le Ste \le 100$).

Fig. 3 shows the isotherms, streamlines and *Cr* contours for the different values of the non-dimensional fusion temperature and the volume fraction of the NEPCM particles. By paying attention to the all streamlines patterns, irrespective of the examined different values of non-dimensional parameters, it is seen that the buoyancy effect and enforced temperature gradient between two differential heating sidewalls induce the convective flow regime inside the porous cavity. Indeed, the nanofluid flow up along the hot wall and makes the single-cell clockwise rotating by flowing down along the cold wall. As mentioned earlier, the *Cr* parameter represents the ratio of the heat capacity of the suspension to that of the host fluid. Thus, the *Cr* contours depict the distribution of heat capacity in the porous region due to the phase change of the nonadecane core inside the nano-encapsulated particles. The red ribbon shape on the *Cr* contours appears around a constant temperature line (isotherm) where their fusion temperature of the phase change of the core can be observed. It is evident that the heat capacity ratio parameter is variable inside the fusion temperature, while it is constant outside the fusion region.

Comparison of Fig. 3a and b demonstrate that increasing the volume fraction of the NEPCM particles from $\phi = 0.02$ to $\phi = 0.05$ for constant θ_f alters the isotherms and the nanofluid flow patterns slightly because of increasing the amount of some fluid properties including the viscosity and the thermal conductivity. Moreover, the red ribbon shape of the *Cr* contour becomes more extensive at the bottom of the enclosure, which enhances the phase change process of the core of the NEPCMs.

Comparison of Fig. 3b and c reveals the impact of normalized fusion temperature on the isotherms, streamlines, and *Cr* fields. An increase in the fusion temperature as $\theta_f = 0.2$ to $\theta_f = 0.5$ changes the isotherms pattern to the horizontal form at the center of the porous cavity. According to the *Cr* contour of Fig. 3, as previously mentioned, the red region of *Cr* contour in which the core-phase change of NEPCMs occurs appears around the temperature distribution line equal with the non-dimensional fusion temperature. The high-temperature gradients in the vicinity of the cold and hot walls cause the phase change area to be thin, while it becomes wider within the center of the porous cavity due to the lower temperature gradients.

Moreover, it can be deduced from the isotherm of Fig. 3b and c that the extension of the isotherm line at the bottom of the cavity toward the hot wall becomes more widespread when the isotherm is identical with θ_f. Thereby, it seems reasonable to conclude that the phase change area is stretched toward the lower insulated wall near the hot wall by increasing the non-dimensional fusion temperature of NEPCM particles. Furthermore, it can be seen that the variation in the non-dimensional fusion temperature leads to change in the streamlines pattern and slightly diminish the flow strength inside the porous cavity.

Fig. 4 is prepared to demonstrate the influence of the Darcy number and the porosity on the isotherms, streamlines, and heat capacity ratio (*Cr*) contours inside the porous cavity. It should be noted that each of the Fig. 4a and b can be individually compared with Fig. 3b (default case of the present study) to investigate the impact of *Da* and ε on the heat transfer and fluid flow characteristics. Comparison of Fig. 3b and a shows that increasing the Darcy number boosts the strength of the nanofluid circulation and forms a rotating double-cell structure in the porous cavity. Indeed, the permeability of the porous medium is the key parameter in the definition of Darcy number, which they have a direct relationship with each other. Therefore, when the Darcy number increases, the nanofluid flow gets intensified in the porous region. The isotherms tend to be almost parallel distribution to the horizontal insulated walls at the high value of the Darcy number (see Fig. 4a), which reveals the strong convection through the porous region.

Furthermore, the red area of *Cr* contour in which the core-phase change process occurs grows broader. This betokens that the heat transfer improves owing to boost the total heat capacity storage of the NEPCM particles. Comparison of Figs. 3b and 4b shows that the streamlines are reinforced as the porosity increases due to the rising of the void space in the porous medium, while it has no significant effects on the isotherms pattern and the phase change phenomena.

The variations of the average Nusselt number versus the non-dimensional fusion temperature for the different values of Stefan number are plotted in Fig. 5. The obtained results reveal that as the Stefan number decreases, the average Nusselt number increases. It is clear from Eq. (21) that the Stefan number has an inverse relation with the latent heat of the NEPCM core. Hence, the low value of *Ste* represents the high latent heat of the NEPCM core. As a consequence, the heat transfer rate boost by increasing the latent heat of the NEPCM core due to increment of the heat storage capacity of the NEPCM particles.

It is worth noticing that the presence of NEPCM particles affects the thermal conductivity, dynamic viscosity, density ratio, and other thermophysical properties of the working fluid. Hence, to observe how heat transfer rate is affected by the core-phase change of nanoparticles, the average Nusselt number is calculated to a case with no phase change. When the latent heat of the NEPCM core approaches zero (the case with no phase change), the Stefan number approaches infinity. Therefore, the average Nusselt number is evaluated for $Ste = 100$, which is a practical value for $Nu_{Ste \to \infty}$. As seen in Fig. 5, in the case of no phase change (i.e., $Ste = 100$), the average Nusselt number is constant as 7.97, whereas the value of average Nusselt number in the case of fluid

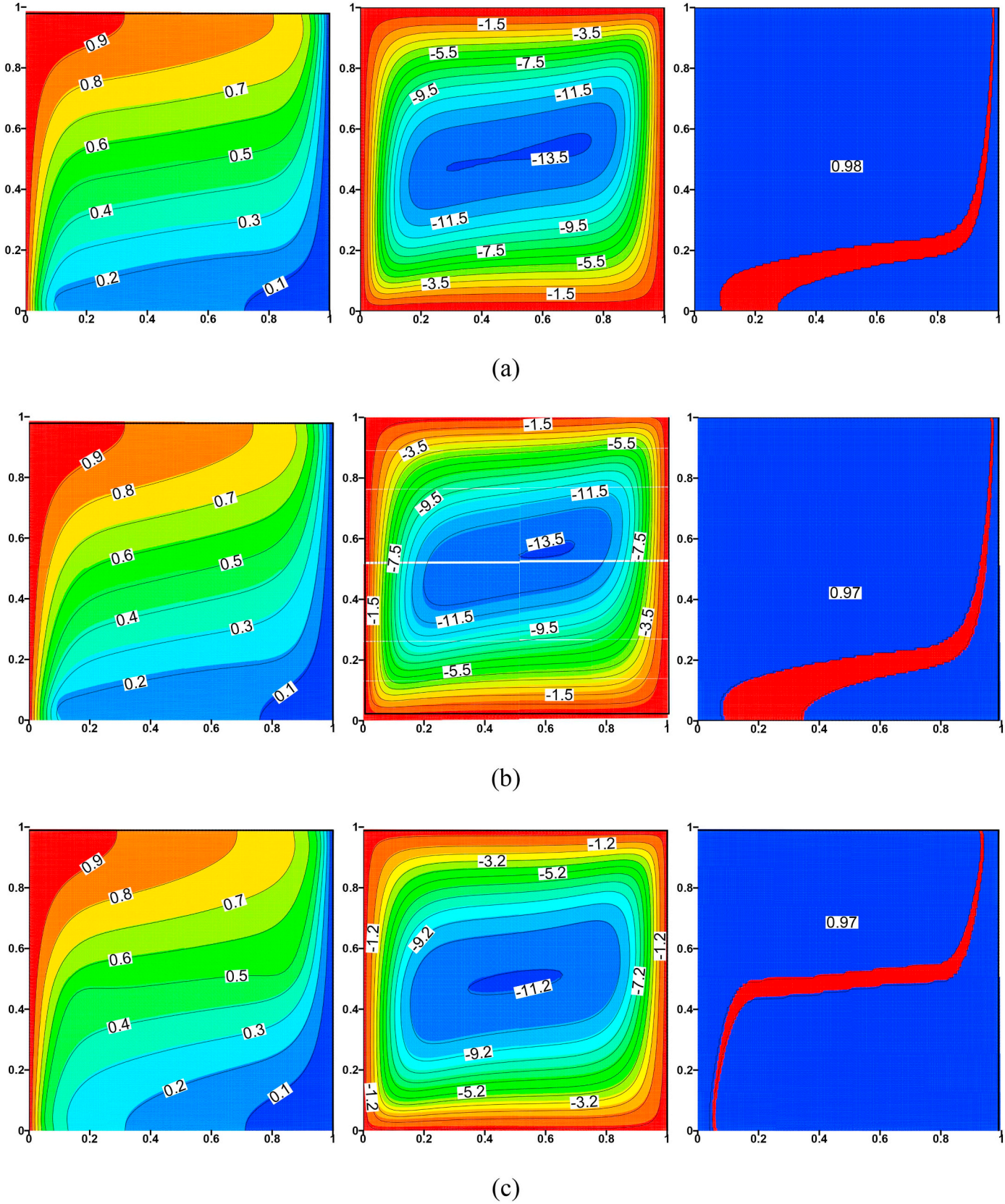

Fig. 3. The isotherms (left side), streamlines (middle) and heat capacity ratio (*Cr*) contours (right side) for; a) $\theta_f = 0.2$, $\phi = 0.02$, b) $\theta_f = 0.2$, $\phi = 0.05$, c) $\theta_f = 0.5$, $\phi = 0.05$.

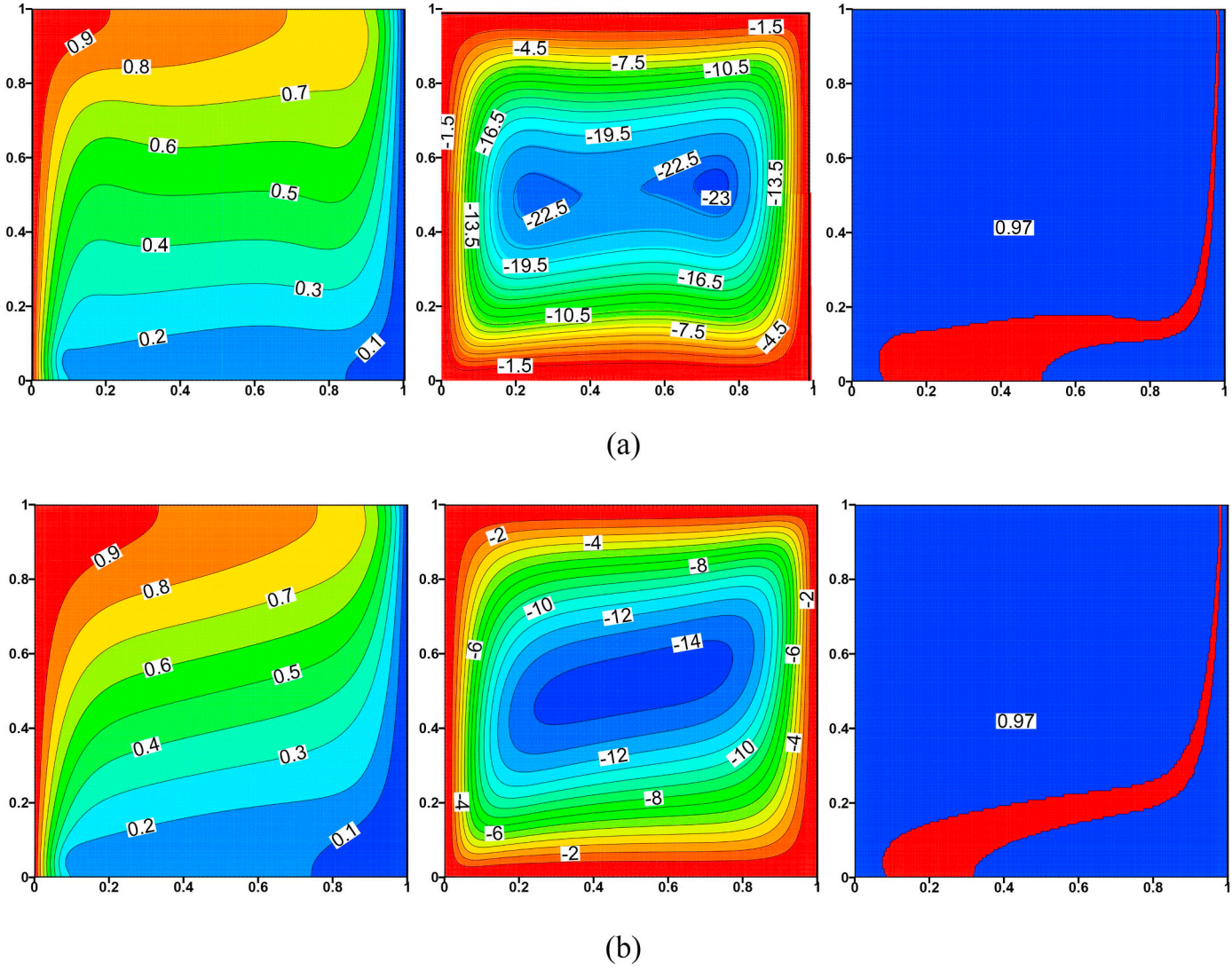

Fig. 4. The isotherms (left side), streamlines (middle) and heat capacity ratio (*Cr*) contours (right side) for; a) $Da = 10^{-2}$, $\varepsilon = 0.65$, and b) $Da = 10^{-3}$, $\varepsilon = 0.9$.

without NEPCM particles (pure fluid) is 7.57. Accordingly, it can be inferred that the presence of nanoparticles solely improves the heat transfer of the natural convection regime inside the porous enclosure.

Further, the depicted results for the average Nusselt number in Fig. 5 show a symmetrical pattern about $\theta_f = 0.5$ for all values of Stefan number. This symmetry is because of the symmetrical studied domain and boundary conditions. The average Nusselt number at $\theta_f = 0.5$ is maximum. As θ_f becomes less or more from 0.5, the average Nusselt number equally decreases. As mentioned earlier (see Fig. 3c), when $\theta_f = 0.5$, the phase change process of the NEPCM core arises in the center of the cavity as well as near the hot and cold sidewalls where the temperature gradients are large. Hence, the maximum average Nusselt number emerges at the optimum fusion temperature, i.e., $\theta_f = 0.5$. As illustrated in Fig. 5, the variations of Nusselt number versus the fusion temperature is a straight line when $Ste = 100$. Indeed, when *Ste* approaches infinity, the phase change occurs immediately, and thus, no heat can be stored in the capsules. Furthermore, the heat capacity ratio, i.e. *Cr*, is no more temperature-dependent, and the fusion temperature has no influence on the rate of heat transfer.

For the sake of investigating the effect of volume fraction of NEPCM particles on the heat transfer rate, the variations of average Nusselt number with the fusion temperature for the various magnitudes of NEPCM particles' volume fraction are provided in Fig. 6. Based on the obtained results, an increase in the volume fraction of NEPCMs boosts the values of the average Nusselt number. By applying 1%, 3%, and 5% of volume fraction of NEPCM particles within the porous cavity at the optimum value of $\theta_f = 0.5$, the heat transfer rate in the form of average Nusselt number respectively augments up to 4.7%, 12.9%, and 20.1% compared to the case with no nanoparticles ($\phi = 0$). When the volume fraction of NEPCM particles is maximum ($\phi = 5\%$) and the dimensionless fusion temperature is optimum ($\theta_f = 0.5$), for $Ra = 10^6$, $Ste = 0.2$, $\varepsilon = 0.65$, and $Da = 10^{-3}$, the average Nusselt number is 9.09. In this case, the augmentation of the heat transfer rate in comparison with the pure fluid ($Nu = 7.57$) and NEPCM mixture with no core-phase change ($Nu = 7.97$) is up to 20.1% and 14.1%, respectively.

Fig. 7 illustrates the simultaneous effects of the Darcy number (*Da*) and the porosity (ε) on the average Nusselt number inside the porous cavity. As expected from the extracted results, the average Nusselt number has an upward trend by increasing the Darcy number at any evaluated value of the porosity. The average Nusselt number rises smoothly in the range $10^{-5} < Da < 10^{-4}$, afterward, the upward trend is followed with a steep slope until about $Da = 10^{-3}$. Finally, the variations of the average Nusselt number are continued with a gentle slope. As mentioned earlier, the high Darcy number represents the high permeability of the porous medium. Obviously, in such a circumstance, the fluid flow gets intensified through the porous cavity. Consequently, the average Nusselt number increases due to the domination of the convection heat transfer regime inside the porous region. Furthermore,

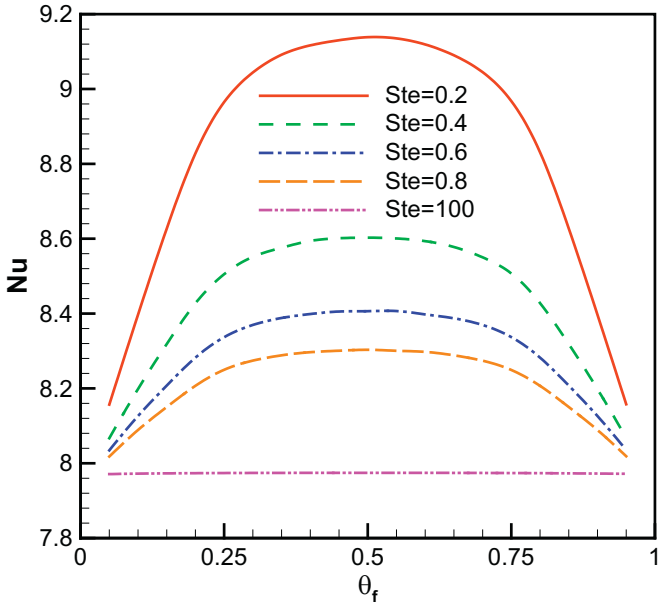

Fig. 5. The variation of average Nusselt number with θ_f for the different values of *Ste*.

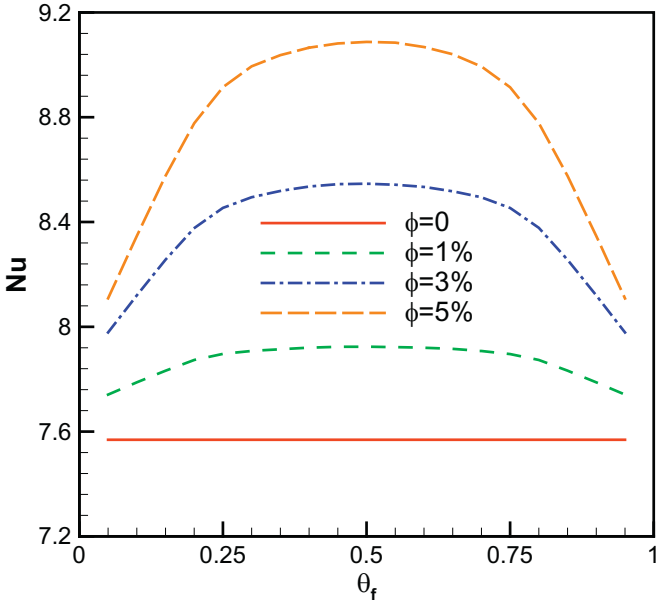

Fig. 6. The variation of average Nusselt number with θ_f for the different values of ϕ.

the average Nusselt number increases with the increment of the porosity, as seen in Fig. 7. This is due to the fact that increase in the porosity leads to increase in the void space, which is saturated by the nanofluid. Hence, the rise of the void space enhances the impact of the presence of NEPCM particles on the effective thermal conductivity. As a result, the heat transfer rate, which is calculated in the form of the average Nusselt number, increases.

5. Conclusion

The numerical investigation of steady natural convection flow and heat transfer in a square porous cavity saturated with a nanofluid was carried out in this paper. The nanofluid was considered as a dilute mixture of NEPCM nanoparticles and the host fluid. To ensure the

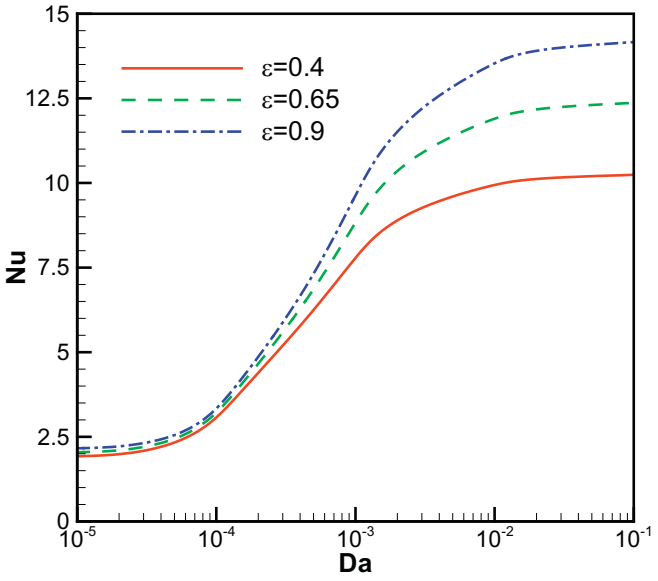

Fig. 7. The variation of average Nusselt number with Darcy number (*Da*) for the different values of porosity (ε).

correctness of the results, the mesh independency was analyzed. We represented the effect of several dimensionless parameters consisting of Darcy number, porosity, Stefan number, fusion temperature, and volume fraction of the NEPCMs on the flow and heat transfer characteristics.

Based on the obtaining results, it can be deduced that using the NEPCM particles enhances the heat transfer due to the augmentation of effective thermal conductivity and heat capacity of the studied nanofluid. Further, the more increase in the volume fraction of NEPCMs leads to more enhancement in the heat transfer rate. The heat transfer rate is seen to be significantly affected by the dimensionless melting temperature. The highest value of *Nu* is derived at θ_f equal to 0.5 which is far enough from the temperature of vertical walls. In this case, the fusion of the PCM cores occurs mostly at the center of the porous cavity. It is also found that the average Nusselt number increases by decreasing the Stefan number. Indeed, the lower Stefan number indicates the higher latent heat of the PCM nucleus. Hence, the increment in the heat capacity of NEPCMs due to higher latent heat leads to enhancement in the heat transfer rate. Eventually, the results showed that *Nu* is an increasing function of the *Da* and ε.

In the present study, we consider that the heat transfer effects of NEPCMs are of interest. However, the energy storage of NEPCMs is another important point of view, with various applications in solar and chemical processes, which can be subject to future studies.

Declaration of Competing Interest

The authors clarify that there is no conflict of interest for report.

References

[1] S. Ostrach, Natural convection in enclosures, Advances in Heat Transfer, Elsevier, 1972, pp. 161–227.
[2] P. Le Quéré, Accurate solutions to the square thermally driven cavity at high Rayleigh number, Comput. Fluids 20 (1) (1991) 29–41.
[3] K. Khanafer, K. Vafai, Isothermal surface production and regulation for high heat flux applications utilizing porous inserts, Int. J. Heat Mass Transf. 44 (15) (2001) 2933–2947.
[4] A. Amiri, K. Vafai, Transient analysis of incompressible flow through a packed bed, Int. J. Heat Mass Transf. 41 (24) (1998) 4259–4279.
[5] D.A. Nield, A. Bejan, Convection in Porous Media, Springer, 2006.
[6] H. Zargartalebi, M. Ghalambaz, M.A. Sheremet, I. Pop, Unsteady free convection in a square porous cavity saturated with nanofluid: the case of local thermal

nonequilibrium and Buongiorno's mathematical models, J. Porous Media 20 (11) (2017) 999–1016.
[7] A.J. Chamkha, A.-R.A. Khaled, Similarity solutions for hydromagnetic mixed convection heat and mass transfer for Hiemenz flow through porous media, Int. J. Num. Methods Heat Fluid Flow 10 (1) (2000) 94–115.
[8] A.J. Chamkha, Hydromagnetic natural convection from an isothermal inclined surface adjacent to a thermally stratified porous medium, Int. J. Eng. Sci. 35 (10 − 11) (1997) 975–986.
[9] P.S. Reddy, A.J. Chamkha, Soret and Dufour effects on MHD convective flow of Al2O3–water and TiO2–water nanofluids past a stretching sheet in porous media with heat generation/absorption, Adv. Powder Technol. 27 (4) (2016) 1207–1218.
[10] A.J. Chamkha, Double-diffusive convection in a porous enclosure with cooperating temperature and concentration gradients and heat generation or absorption effects, Numerical Heat Transfer 41 (1) (2002) 65–87.
[11] M. Modather, A. CHAMKHA, An analytical study of MHD heat and mass transfer oscillatory flow of a micropolar fluid over a vertical permeable plate in a porous medium, Turk. J. Eng. Environ. Sci. 33 (4) (2010) 245–258.
[12] P. Keblinski, J.A. Eastman, D.G. Cahill, Nanofluids for thermal transport, Mater. Today 8 (6) (2005) 36–44.
[13] W. Su, J. Darkwa, G. Kokogiannakis, Review of solid–liquid phase change materials and their encapsulation technologies, Renew. Sust. Energ. Rev. 48 (2015) 373–391.
[14] M.M. Farid, A.M. Khudhair, S.A.K. Razack, S. Al-Hallaj, A review on phase change energy storage: materials and applications, Energy Convers. Manag. 45 (9–10) (2004) 1597–1615.
[15] G. Fang, H. Li, F. Yang, X. Liu, S. Wu, Preparation and characterization of nano-encapsulated n-tetradecane as phase change material for thermal energy storage, Chem. Eng. J. 153 (1–3) (2009) 217–221.
[16] J.-K. Choi, J.G. Lee, J.H. Kim, H.-s. Yang, Preparation of microcapsules containing phase change materials as heat transfer media by in-situ polymerization, J. Ind. Eng. Chem. 7 (6) (2001) 358–362.
[17] C. Alkan, A. Sarı, A. Karaipekli, Preparation, thermal properties and thermal reliability of microencapsulated n-eicosane as novel phase change material for thermal energy storage, Energy Convers. Manag. 52 (1) (2011) 687–692.
[18] M. You, X. Zhang, J. Wang, X. Wang, Polyurethane foam containing micro-encapsulated phase-change materials with styrene–divinybenzene co-polymer shells, J. Mater. Sci. 44 (12) (2009) 3141–3147.
[19] M. You, X. Wang, X. Zhang, L. Zhang, J. Wang, Microencapsulated n-Octadecane with styrene-divinybenzene co-polymer shells, J. Polym. Res. 18 (1) (2011) 49–58.
[20] X. Qiu, W. Li, G. Song, X. Chu, G. Tang, Fabrication and characterization of microencapsulated n-octadecane with different crosslinked methylmethacrylate-based polymer shells, Sol. Energy Mater. Sol. Cells 98 (2012) 283–293.
[21] A. Jamekhorshid, S. Sadrameli, M. Farid, A review of microencapsulation methods of phase change materials (PCMs) as a thermal energy storage (TES) medium, Renew. Sust. Energ. Rev. 31 (2014) 531–542.
[22] K. Pielichowska, K. Pielichowski, Phase change materials for thermal energy storage, Prog. Mater. Sci. 65 (2014) 67–123.
[23] A.N. Keshteli, M. Sheikholeslami, Nanoparticle enhanced PCM applications for intensification of thermal performance in building: a review, J. Mol. Liq. 274 (2018) 516–533.
[24] V.V. Tyagi, D. Buddhi, PCM thermal storage in buildings: a state of art, Renew. Sust. Energ. Rev. 11 (6) (2007) 1146–1166.
[25] Y. Rabin, I. Bar-Niv, E. Korin, B. Mikic, Integrated solar collector storage system based on a salt-hydrate phase-change material, Sol. Energy 55 (6) (1995) 435–444.
[26] P. Moreno, C. Solé, A. Castell, L.F. Cabeza, The use of phase change materials in domestic heat pump and air-conditioning systems for short term storage: a review, Renew. Sust. Energ. Rev. 39 (2014) 1–13.
[27] R. Hossain, S. Mahmud, A. Dutta, I. Pop, Energy storage system based on nanoparticle-enhanced phase change material inside porous medium, Int. J. Therm. Sci. 91 (2015) 49–58.
[28] M. Sheikholeslami, Numerical modeling of Nano enhanced PCM solidification in an enclosure with metallic fin, J. Mol. Liq. 259 (2018) 424–438.
[29] N. Bondareva, M. Sheremet, Natural convection melting of nano-enhanced phase change material in a cavity with finned copper profile, MATEC Web of Conferences, EDP Sciences, 2018.
[30] M. Ghalambaz, A. Doostani, E. Izadpanahi, A. Chamkha, Phase-change heat transfer in a cavity heated from below: the effect of utilizing single or hybrid nanoparticles as additives, J. Taiwan Inst. Chem. Eng. 72 (2017) 104–115.
[31] S. Hosseini, M. Sheikholeslami, M. Ghasemian, D. Ganji, Nanofluid heat transfer analysis in a microchannel heat sink (MCHS) under the effect of magnetic field by means of KKL model, Powder Technol. 324 (2018) 36–47.
[32] A. Chamkha, A. Doostanidezfuli, E. Izadpanahi, M. Ghalambaz, Phase-change heat transfer of single/hybrid nanoparticles-enhanced phase-change materials over a heated horizontal cylinder confined in a square cavity, Adv. Powder Technol. 28 (2) (2017) 385–397.
[33] R. Elbahjaoui, H. El Qarnia, Transient behavior analysis of the melting of nano-particle-enhanced phase change material inside a rectangular latent heat storage unit, Appl. Therm. Eng. 112 (2017) 720–738.
[34] H.R. Seyf, M.R. Wilson, Y. Zhang, H. Ma, Flow and heat transfer of nanoencapsulated phase change material slurry past a unconfined square cylinder, J. Heat Transf. 136 (5) (2014) 051902.
[35] H.R. Seyf, Z. Zhou, H. Ma, Y. Zhang, Three dimensional numerical study of heat-transfer enhancement by nano-encapsulated phase change material slurry in microtube heat sinks with tangential impingement, Int. J. Heat Mass Transf. 56 (1–2) (2013) 561–573.
[36] C.-J. Ho, W.-C. Chen, W.-M. Yan, Experimental study on cooling performance of minichannel heat sink using water-based MEPCM particles, Int. Commun. Heat Mass Transfer 48 (2013) 67–72.
[37] C.-J. Ho, W.-C. Chen, W.-M. Yan, Correlations of heat transfer effectiveness in a minichannel heat sink with water-based suspensions of Al2O3 nanoparticles and/or MEPCM particles, Int. J. Heat Mass Transf. 69 (2014) 293–299.
[38] C.-J. Ho, J. Huang, P. Tsai, Y.M. Yang, Water-based suspensions of Al2O3 nanoparticles and MEPCM particles on convection effectiveness in a circular tube, Int. J. Therm. Sci. 50 (5) (2011) 736–748.
[39] M. Ghalambaz, A.J. Chamkha, D. Wen, Natural convective flow and heat transfer of Nano-encapsulated phase change materials (NEPCMs) in a cavity, Int. J. Heat Mass Transf. 138 (2019) 738–749.
[40] A. Hajjar, S. Mehryan, M. Ghalambaz, Time periodic natural convection heat transfer in a nano-encapsulated phase-change suspension, Int. J. Mech. Sci. (2019) 105243.
[41] M. Ghalambaz, T. Groşan, I. Pop, Mixed convection boundary layer flow and heat transfer over a vertical plate embedded in a porous medium filled with a suspension of nano-encapsulated phase change materials, J. Mol. Liq. 293 (2019) 111432.
[42] S. Barlak, O.N. Sara, A. Karaipekli, S. Yapıcı, Thermal conductivity and viscosity of nanofluids having nanoencapsulated phase change material, Nanoscale Microscale Thermophys. Eng. 20 (2) (2016) 85–96.
[43] M. Ghalambaz, M.A. Sheremet, I. Pop, Free convection in a parallelogrammic porous cavity filled with a nanofluid using Tiwari and Das' nanofluid model, PLoS One 10 (5) (2015) e0126486.
[44] L. Chai, R. Shaukat, L. Wang, H.S. Wang, A review on heat transfer and hydrodynamic characteristics of nano/microencapsulated phase change slurry (N/MPCS) in mini/microchannel heat sinks, Appl. Therm. Eng. 135 (2018) 334–349.
[45] B. Chen, X. Wang, R. Zeng, Y. Zhang, X. Wang, J. Niu, Y. Li, H. Di, An experimental study of convective heat transfer with microencapsulated phase change material suspension: laminar flow in a circular tube under constant heat flux, Exp. Thermal Fluid Sci. 32 (8) (2008) 1638–1646.
[46] K. Khanafer, K. Vafai, A critical synthesis of thermophysical characteristics of nanofluids, Int. J. Heat Mass Transf. 54 (19–20) (2011) 4410–4428.
[47] A. Zaraki, M. Ghalambaz, A.J. Chamkha, M. Ghalambaz, D. De Rossi, Theoretical analysis of natural convection boundary layer heat and mass transfer of nanofluids: effects of size, shape and type of nanoparticles, type of base fluid and working temperature, Adv. Powder Technol. 26 (3) (2015) 935–946.
[48] M. Ghalambaz, A. Doostani, E. Izadpanahi, A.J. Chamkha, Phase-change heat transfer in a cavity heated from below: the effect of utilizing single or hybrid nanoparticles as additives, J. Taiwan Inst. Chem. Eng. 72 (2017) 104–115.
[49] The Finite Element Method for Fluid Dynamics, in: O.C. Zienkiewicz, R.L. Taylor, P. Nithiarasu (Eds.), The Finite Element Method for Fluid Dynamics (Seventh Edition), Butterworth-Heinemann, Oxford, 2014, p. iii.
[50] K. Kahveci, Buoyancy driven heat transfer of nanofluids in a tilted enclosure, J. Heat Transf. 132 (6) (2010) 062501.
[51] Q. Sun, I. Pop, Free convection in a triangle cavity filled with a porous medium saturated with nanofluids with flush mounted heater on the wall, Int. J. Therm. Sci. 50 (11) (2011) 2141–2153.
[52] M.A. Sheremet, T. Grosan, I. Pop, Free convection in a square cavity filled with a porous medium saturated by nanofluid using Tiwari and Das' nanofluid model, Transp. Porous Media 106 (3) (2015) 595–610.
[53] O. Turan, A. Sachdeva, N. Chakraborty, R.J. Poole, Laminar natural convection of power-law fluids in a square enclosure with differentially heated side walls subjected to constant temperatures, J. Non-Newtonian Fluid Mech. 166 (17) (2011) 1049–1063.